Electronics and Communications in Japan, Part 3, Vol. 85, No. 2, 2002
Translated from Denshi Joho Tsushin Gakkai Ronbunshi, Vol. J84-A, No. 1, January 2001, pp. 13–21

Wavelet-Based Image Coding Using All-Pass Filters

Seiya Kamimura, Xi Zhang, and Toshinori Yoshikawa

Department of Electrical Engineering, Nagaoka University of Technology, Nagaoka, Niigata, 940-2188 Japan

SUMMARY

FIR wavelet filters are mainly used in conventional wavelet-based image coding. However, FIR filters, except for the Haar wavelet, cannot satisfy both the exactly linear phase and orthonormality conditions. For example, the well-known Daubechies-9/7 wavelet is biorthogonal. In this paper, an effective implementation of the all-pass-based wavelet filters is presented for wavelet-based image coding. Since all-pass filters are IIR, both the exactly linear phase and orthonormality conditions can be simultaneously satisfied, so that better compression performance can be expected. Also, IIR filters can be realized with a lower computational complexity than can FIR filters. Finally, the proposed IIR wavelet filters are evaluated by using SPIHT to compress the practical images, and the influence of the all-pass filters and delay elements on the compression performance is investigated. It is shown through the experimental results that the IIR wavelet filters proposed in this paper have a lower computational complexity than the Daubechies-9/7 wavelet, with a comparable compression performance. © 2001 Scripta Technica, Electron Comm Jpn Pt 3, 85(2): 13–21, 2002

Key words: Image compression; wavelet; all-pass filter; IIR filter.

1. Introduction

In the past decade, wavelet-based image coding has been extensively studied and applied in JPEG and MPEG [1–13]. In the wavelet-based image coding scheme, two-band PR (perfect reconstruction) filter banks play a very important role. To avoid redundancy between subimages, the orthonormality condition is required for two-band PR filter banks. In addition, the analysis and synthesis filters are required to have an exactly linear phase response, since the symmetric extension method is generally used to accurately handle the boundaries of finite-length signals [5]. Unfortunately, these two conditions cannot be simultaneously satisfied by conventional FIR wavelet filters, except for the Haar wavelet [1]. The Haar wavelet is discontinuous and is not suitable for compression of natural images [6, 13]. Thus, more regularity than the Haar wavelet is necessary in compression of natural images. For example, the Daubechies-9/7 wavelet abandons the orthonormality condition to get more regularity [6]. That is, the Daubechies-9/7 wavelet is biorthogonal. On the other hand, a class of IIR wavelet filters has been constructed by using all-pass filters in Ref. 8, where these two conditions are simultaneously satisfied. In the design of IIR wavelet filters, the design method for the maximally flat filters has been proposed in Refs. 11 and 12, and a closed-form solution has been given. In Ref. 12, a method for designing filters with arbitrary flatness has also been presented, and the influence of the delay elements on the frequency response has been investigated.

In this paper, we present an effective implementation of the all-pass-based IIR wavelet filters for wavelet-based image coding. By using IIR filters, both the exactly linear phase and orthonormality conditions can be simultaneously satisfied, making better compression performance likely. Furthermore, IIR filters have a lower computational complexity in implementation and more degrees of freedom in design than FIR filters. Finally, the proposed IIR wavelet filters are evaluated by using SPIHT to compress the practical images, and the influence of the order of all-pass filters and delay elements on the compression performance is

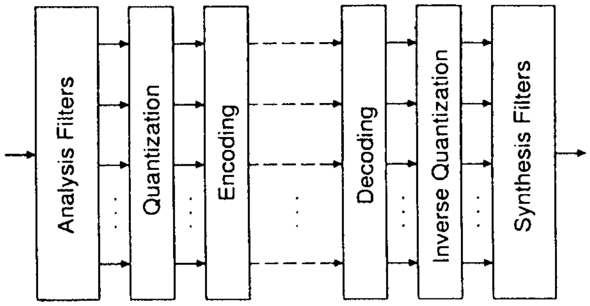

Fig. 1. Subband coding.

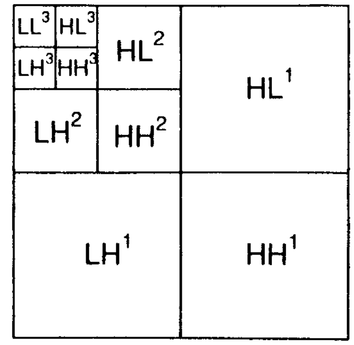

Fig. 3. 2D decomposition.

investigated. Also, both the compression performance and computational complexity are compared with the well-known Daubechies-9/7 wavelet.

2. Wavelet-Based Image Coding

First, we describe the principle of subband coding shown in Fig. 1. In the analysis stage, an input signal is decomposed into subband signals by analysis filters. The resulting subband signals are separately quantized and then entropy-encoded. In the synthesis stage, the compressed subband signals are decoded, then the signal is reconstructed by synthesis filters. Here, the aim of the subband coding is to minimize the difference between the original and reconstructed signals with the given compression rate, or to maximize the compression rate within the given error.

In the wavelet-based image coding scheme, two-band PR filter banks play a very important role. The input signal is decomposed into low- and high-frequency components by a two-band filter bank. Next, the low-frequency component is similarly decomposed by using the same filter bank. By iteration on the low-frequency component, octave decomposition is obtained. For example, decomposition up to three levels in one dimension is shown in Fig. 2. In the synthesis stage, the process is performed in the reverse order of that in the analysis stage. In two-dimension cases such as images, decomposition is done separately in the horizontal and vertical directions, and four-subband images are obtained. Next, the same process is iterated on the low-frequency component. Figure 3 is an example of decomposition up to three level in two dimensions.

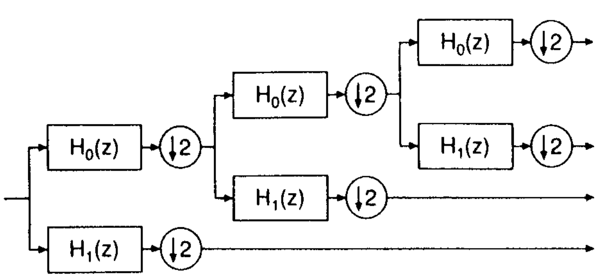

Fig. 2. Wavelet decomposition.

3. All-Pass-Based Wavelet Filters

3.1. Design of IIR Wavelet Filters

In the wavelet-based image coding scheme, two-band PR filter banks play a very important role. To avoid redundancy between subimages, the orthonormality condition is required for two-band PR filter banks. In addition, the analysis and synthesis filters are required to have an exactly linear phase response, since the symmetric extension method is generally used to accurately handle the boundaries of images [5]. Unfortunately, these two conditions cannot be simultaneously satisfied by the conventional FIR wavelet filters, except for the Haar wavelet. The Haar wavelet is discontinuous and thus is not suitable for compression of natural images [6, 13]. Therefore, a greater regularity than the Haar wavelet is necessary for compression of natural images. For example, the Daubechies-9/7 wavelet abandons the orthonormality condition to get more regularity. On the other hand, these two conditions can be simultaneously satisfied by IIR filters [8]. The orthonormality condition that wavelet filters must satisfy is

$$\begin{cases} H_0(z)H_0(z^{-1}) + H_0(-z)H_0(-z^{-1}) = 1 \\ H_1(z)H_1(z^{-1}) + H_1(-z)H_1(-z^{-1}) = 1 \\ H_0(z)H_1(z^{-1}) + H_0(-z)H_1(-z^{-1}) = 0 \end{cases} \tag{1}$$

where $H_0(z)$ is a low-pass filter and $H_1(z)$ is a high-pass filter. In Refs. 8, 11, and 12, $H_0(z)$ and $H_1(z)$ are constructed by all-pass filters as follows:

$$\begin{cases} H_0(z) = \frac{1}{2}\{A(z^2) + z^{-2K-1}A(z^{-2})\} \\ H_1(z) = \frac{1}{2}\{A(z^2) - z^{-2K-1}A(z^{-2})\} \end{cases} \tag{2}$$

where K is an integer, and the all-pass filter $A(z)$ of order N is defined by

$$A(z) = z^{-N} \frac{\sum_{n=0}^{N} a_n z^n}{\sum_{n=0}^{N} a_n z^{-n}} \tag{3}$$

where filter coefficients a_n are real. Assume that $\theta(\omega)$ is the phase response of $A(z)$, that is,

$$\theta(\omega) = -N\omega + 2\tan^{-1} \frac{\sum_{n=0}^{N} a_n \sin n\omega}{\sum_{n=0}^{N} a_n \cos n\omega} \tag{4}$$

Then the frequency responses of $H_0(z)$ and $H_1(z)$ are

$$\begin{cases} H_0(e^{j\omega}) = e^{-j\frac{2K+1}{2}\omega} \cos\left[\theta(2\omega) + \left(K + \frac{1}{2}\omega\right)\right] \\ H_1(e^{j\omega}) = je^{-j\frac{2K+1}{2}\omega} \sin\left[\theta(2\omega) + \left(K + \frac{1}{2}\omega\right)\right] \end{cases} \tag{5}$$

It is clear that an exactly linear phase response is obtained. Also, $H_0(z)$ and $H_1(z)$ in Eq. (2) satisfy the orthonormality condition of Eq. (1). That is, $H_0(z)$ and $H_1(z)$ have a power-complementary relation:

$$|H_0(e^{j\omega})|^2 + |H_1(e^{j\omega})|^2 = 1 \tag{6}$$

Since $H_0(z)$ and $H_1(z)$ are designed as a pair of low-pass and high-pass filters, the desired phase response of $A(z)$ is

$$\theta_d(\omega) = -\frac{2K+1}{4}\omega \qquad (0 \leqq \omega \leqq 2\omega_p) \tag{7}$$

where ω_p is the band edge frequency of the passband of $H_0(z)$. A flat frequency response is required from the regularity of the wavelets. For the maximally flat filters, the filter coefficients a_i can be analytically determined [11, 12]. The closed form solution is given by

$$a_n = (-1)^n \binom{N}{n} \prod_{i=1}^{n} \frac{i - 1 - N + \frac{K}{2} + \frac{1}{4}}{i + \frac{K}{2} + \frac{1}{4}} \tag{8}$$

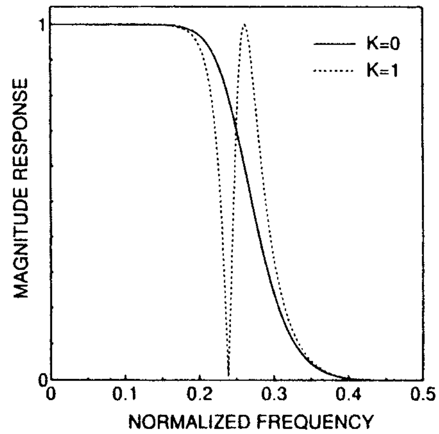

Fig. 4. Magnitude responses of $H_0(z)$ ($N = 2$).

It has been pointed out in Ref. 12 that the magnitude response has an undesired ripple in the transition band, as shown in Fig. 4, when the order N of the all-pass filter is even and the order of delay elements is $K = 4k + 1$ or $4k + 2$. When N is odd and $K = 4k$ or $4k + 3$, there is similarly an undesired ripple. To avoid this problem, we should choose $K = 4k$ or $4k + 3$ when N is even, and $K = 4k + 1$ or $4k + 2$ when N is odd, where $k = 0, 1, \ldots, \lfloor \frac{N}{2} \rfloor$.

3.2. Implementation of IIR Wavelet Filters

In this section, we present an effective implementation of the IIR wavelet filters proposed in Section 3.1 for wavelet-based image coding. The transfer functions in Eq. (2) can be realized in the polyphase structure shown in Fig. 5 [2]. In the following, we describe the implementation of the IIR wavelet filters using the polyphase structure in Fig. 5. First, we assume that $x(n)$ is an input signal of length M, and that $\tilde{x}(n)$ is a periodic signal of period $2M$ obtained by employing the symmetric extension method, whose z trans-

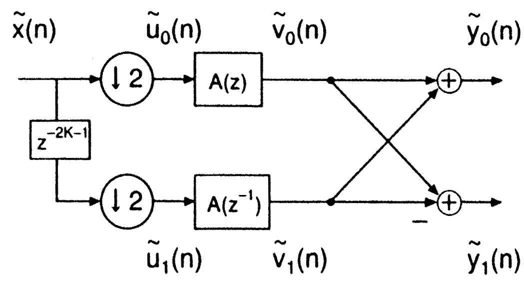

Fig. 5. All-pass-based filter banks.

form is $\tilde{X}(z)$. In the following, a lowercase letter means a time-domain signal, an uppercase letter is its z transform, and a superscript tilde denotes a periodic signal. Next, we demonstrate the decomposition process by the example of $M = 8$ and $K = 0$. As shown in Fig. 6, $\tilde{x}(n)$ is first decimated to get periodic signals $\tilde{u}_0(n)$ and $\tilde{u}_1(n)$ with period M. It is seen in Fig. 6 that $\tilde{u}_0(n)$ and $\tilde{u}_1(n)$ can be gotten just by rearranging $x(n)$ in even and odd order. Then, we have the following symmetrical relation:

$$\tilde{u}_0(n) = \tilde{u}_1(M - 1 - n) \tag{9}$$

that is,

$$\tilde{U}_0(z) = z^{-M+1}\tilde{U}_1(z^{-1}) \tag{10}$$

When $K \neq 0$, the even samples of the signal are eliminated if K is even, and the odd samples are eliminated if K is odd. In every case, the symmetric relation still holds, although the symmetry point may be different. In general, $\tilde{u}_0(n)$ and $\tilde{u}_1(n)$ should be passed through $A(z)$ and $A(z^{-1})$ to get $\tilde{v}_0(n)$ and $\tilde{v}_1(n)$, respectively. That is,

$$\begin{aligned} \tilde{V}_0(z) &= A(z)\tilde{U}_0(z) \\ \tilde{V}_1(z) &= A(z^{-1})\tilde{U}_1(z) \end{aligned} \tag{11}$$

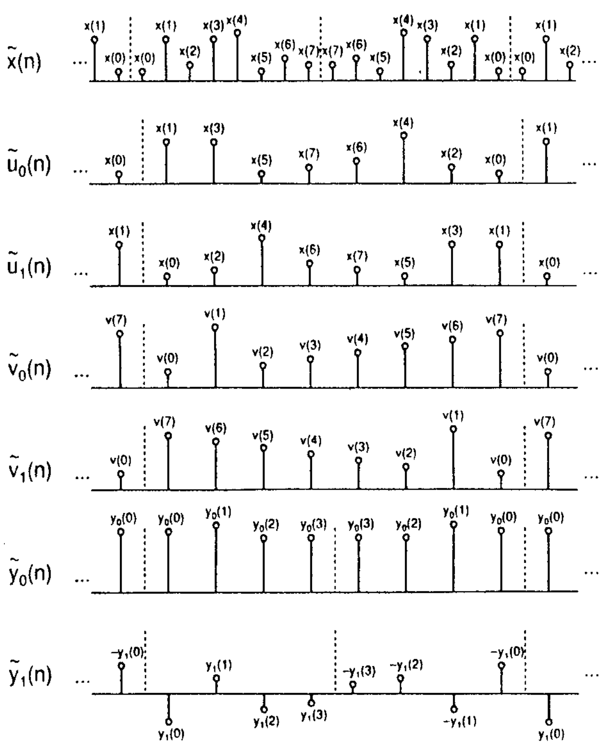

Fig. 6. Decomposition process.

Thus, from Eq. (11)

$$\tilde{V}_0(z) = z^{-M+1}\tilde{V}_1(z^{-1}) \tag{12}$$

that is,

$$\tilde{v}_0(n) = \tilde{v}_1(M - 1 - n) \tag{13}$$

The subband signals $\tilde{y}_0(n)$ and $\tilde{y}_1(n)$ can be obtained by

$$\begin{cases} \tilde{y}_0(n) = \tilde{v}_0(n)+\tilde{v}_1(n) = \tilde{v}_0(n)+\tilde{v}_0(M-1-n) \\ \tilde{y}_1(n) = \tilde{v}_0(n)-\tilde{v}_1(n) = \tilde{v}_0(n)-\tilde{v}_0(M-1-n) \end{cases} \tag{14}$$

which are dependent on $\tilde{v}_0(n)$ only. Therefore, we just need to pass $\tilde{u}_0(n)$ through $A(z)$ to get $\tilde{v}_0(n)$.

Next, we describe the implementation of all-pass filters $A(z)$. In general, $A(z)$ is composed of first- and second-order all-pass filters with real coefficients. In this paper, we will use the maximally flat all-pass filters $A(z)$ for image compression. The maximally flat filters are found to be composed of first-order all-pass filters only:

$$A(z) = \prod_{i=1}^{N} A_i(z) = \prod_{i=1}^{N} \frac{z^{-1} - \alpha_i}{1 - \alpha_i z^{-1}} \tag{15}$$

where α_i is a pole of the filter, and is real. The maximally flat filters designed in Ref. 12 are generally noncausal, and their poles lie inside and outside the unit circle. Noncausal all-pass filters can be divided into $A^S(z)$ and $A^U(z)$, which have the poles located inside and outside the unit circle, respectively. $A^U(z^{-1})$ then becomes

$$A^U(z^{-1}) = \prod_{i=1}^{N_1} \frac{z^{-1} - \dfrac{1}{\alpha_i}}{1 - \dfrac{1}{\alpha_i} z^{-1}} \tag{16}$$

which is causal stable. Therefore, $A^U(z)$ can be realized by reversing the input signal, passing it through causal stable $A^U(z^{-1})$, and then re-reversing the output signal, as shown in Fig. 7.

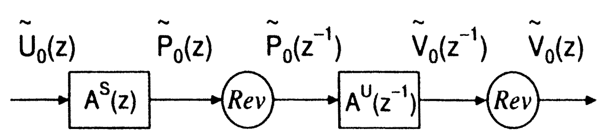

Fig. 7. Cascade of all-pass filters.

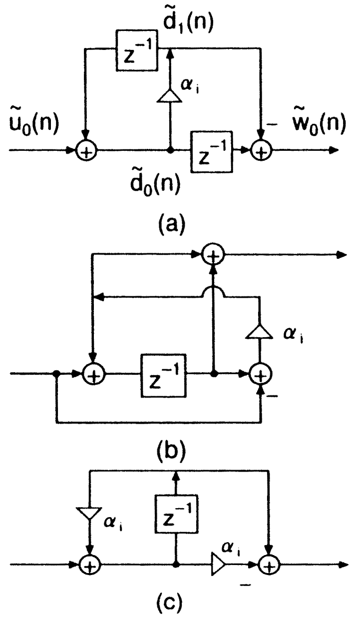

Fig. 8. Structure of first-order all-pass filters.

Since the all-pass filters are composed of first-order all-pass filters only, we consider the implementation of first-order all-pass filters. Typical structures of first-order all-pass filters are shown in Fig. 8. These three structures should be chosen according to the practical application, because the numbers of multipliers, adders, and delay elements required in these structures are different. In this paper, we choose the structure in Fig. 8(a) by considering the computational complexity. Its input–output relation is given by

$$\begin{cases} \tilde{d}_0(n) = \tilde{u}_0(n) + \tilde{d}_1(n-1) \\ \tilde{d}_1(n) = \alpha_i \tilde{d}_0(n) \\ \tilde{w}_0(n) = \tilde{d}_0(n-1) - \tilde{d}_1(n) \end{cases} \tag{17}$$

where only one multiplier and two adders are needed. Since the input signal is periodic, we need to compute initial values $\tilde{d}_0(-1)$ and $\tilde{d}_1(-1)$. These initial values can be computed by

$$\begin{aligned} \tilde{d}_0(-1) &= \tilde{u}_0(-1) + \alpha_i \tilde{u}_0(-2) + \alpha_i^2 \tilde{u}_0(-3) \\ &\quad + \cdots + \alpha_i^{L-1} \tilde{u}_0(-L) \\ &= \tilde{u}_0(-1) + \alpha_i\{\tilde{u}_0(-2) + \alpha_i\{\tilde{u}_0(-3) + \\ &\quad \cdots + \alpha_i\{\tilde{u}_0(-L+1) + \alpha_i \tilde{u}_0(-L)\}\cdots\}\} \end{aligned} \tag{18}$$

Table 1. Comparison of computational complexity

Filter Type	N_M	N_A
All-pass-2	2.08	5.07
All-pass-3	3.12	7.11
All-pass-4	4.16	9.15
Daubechies-9/7	4.50	7.00

$$\tilde{d}_1(-1) = \alpha_i \tilde{d}_0(-1) \tag{19}$$

Although L must be $L \to \infty$ in theory, a large L is sufficient in practice. Experientially, the error caused by the initial values becomes sufficiently small for $L = 20$ to 40. Taking the computation of the initial values into account, the number of multiplications and additions required for first-order all-pass filters are $1 + \frac{L}{M}$ and $2 + \frac{L-1}{M}$, respectively. Therefore, the number of multiplications N_M and the number of additions N_A required in the wavelet filters composed of all-pass filters of order N are

$$\begin{aligned} N_M &= N\left(1 + \frac{L}{M}\right) \\ N_A &= N\left(2 + \frac{L-1}{M}\right) + 1 \end{aligned} \tag{20}$$

For example, the computational complexity required in the case of $M = 512$, $L = 20$, $N = 2$ to 4 is given in Table 1.

4. Experimental Results

To evaluate the proposed IIR wavelet filters, we decompose images up to level 6, and then use the SPIHT proposed in Ref. 10 to compress the practical images. To save coding/decoding time, we have used the binary-uncoded version of the SPIHT without arithmetical coding. It was pointed out in Ref. 10 that the peak signal-to-noise ratio (PSNR) can be improved by about 0.3 to 0.6 dB with arithmetical coding, but at the expense of a larger execution time. The images Barbara, Lena, Boat, and Goldhill of size 512 × 512, 8 bpp are used as test images. The distortion is measured by the PSNR between the original and reconstructed images. The IIR wavelet filters used here are the maximally flat filters.

4.1. Influence of the delay order

It has been pointed out in Section 3.1 that the magnitude responses of the filters are strongly influenced by the delay order K. Here, we investigate the influence of K on the compression performance. The results of Barbara obtained with $N = 2$ and $N = 3$ are shown in Figs. 9 and 10, respectively. It is seen that when N is even, $K = 0$ and $K = 3$ have a better result than $K = 1$ and $K = 2$, while $K = 1$ and $K = 2$ are better when N is odd. It is thought to be due to the influence of the undesired ripple in the transition band described in Section 3.1. Also, the compression performance becomes worse with increasing K. Therefore, we conclude that the optimal K is $K = 0$ or 3 when N is even, and $K = 1$ or 2 when N is odd. In the following, we choose $K = 0$ for even N and $K = 1$ for odd N.

4.2. Influence of the all-pass filter order

The regularity of wavelets increases with increasing order N of the all-pass filters, but the computational complexity becomes larger. Thus, it is necessary to investigate the influence of the filter order on the compression performance. The results for Barbara are shown in Fig. 11, where $N = 0$ corresponds to the conventional Haar wavelet. It is seen that the compression performance shows little improvement when the filter order is above $N = 4$, so that $N = 3$ or $N = 4$ is best. The results for Lena are shown in Fig. 12. In the case of Lena, since there are many low-frequency components, the performance does not improve above $N = 3$. Therefore, we conclude that $N = 2$ or $N = 3$ is sufficient for most natural images with predominantly smooth background such as Lena, and $N = 3$ or $N = 4$ for natural images with high-frequency components such as Barbara.

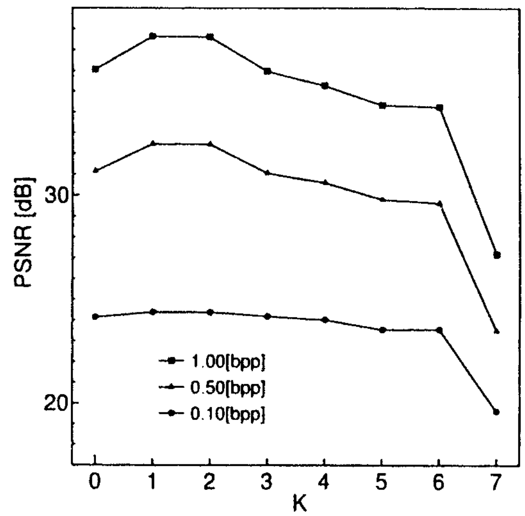

Fig. 10. Influence of delay order K ($N = 3$).

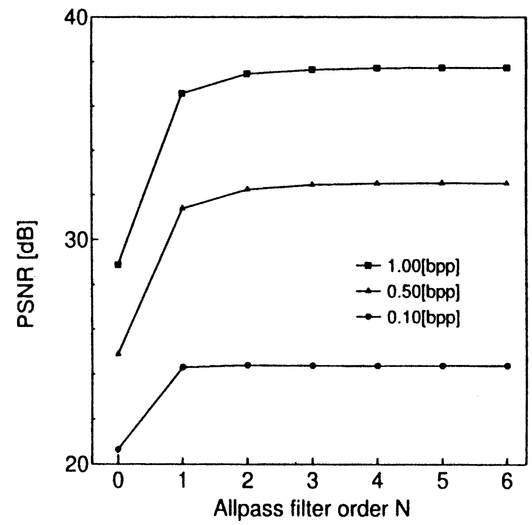

Fig. 11. Influence of all-pass filter order N (Barbara).

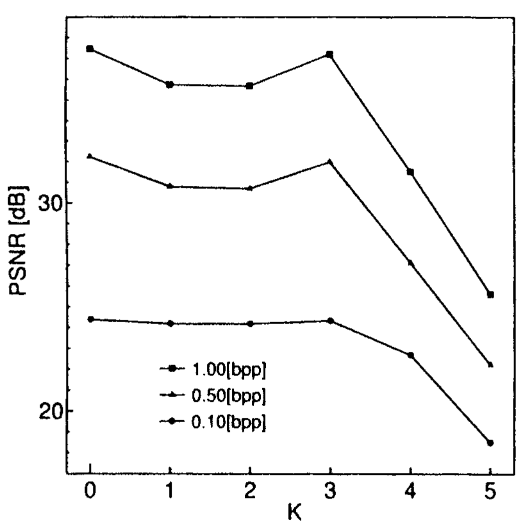

Fig. 9. Influence of delay order K ($N = 2$).

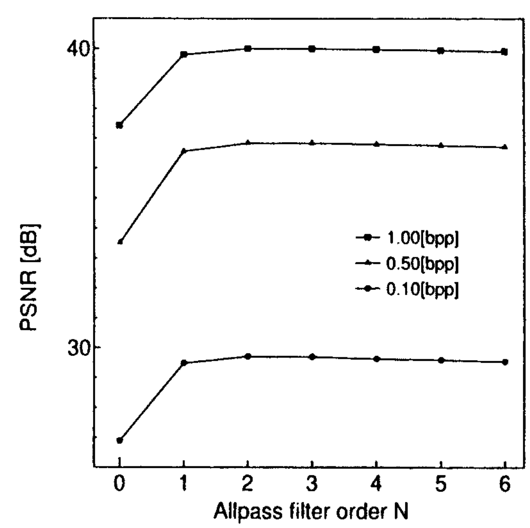

Fig. 12. Influence of all-pass filter order N (Lena).

Fig. 13. Original image (Barbara).

Table 2. Comparison of coding performance (PSNR in dB)

Image	bpp	All-2	All-3	All-4	D-9/7
Boat	1.000	**38.36**	38.32	38.25	38.34
	0.500	**33.81**	33.78	33.74	33.74
	0.250	30.29	30.27	30.22	**30.34**
	0.125	27.55	27.53	27.48	**27.70**
Goldhill	1.000	35.90	**35.91**	35.89	35.86
	0.500	32.55	32.54	32.52	**32.57**
	0.250	30.04	30.03	30.01	**30.16**
	0.125	**28.24**	28.21	28.19	28.18
Lena	1.000	**39.99**	**39.99**	39.97	39.90
	0.500	36.83	**36.84**	36.80	36.74
	0.250	33.72	**33.74**	33.69	33.62
	0.125	**30.68**	30.67	30.60	30.61
Barbara	1.000	37.46	37.64	**37.71**	36.79
	0.500	32.24	32.45	**32.51**	31.60
	0.250	28.05	28.17	**28.19**	27.60
	0.125	24.95	**24.97**	24.90	24.89

4.3. Comparison with the conventional wavelets

In this section, the IIR wavelet filters with $N = 2, 3, 4$ proposed in this paper are compared with the conventional FIR wavelet filters. We chose the Daubechies-9/7 wavelet as a comparison object since it is thought to be among the best wavelet bases in the case of lossy compression [13]. The comparison of the computational complexity is shown in Table 1. It is clear that the wavelet filters with $N = 2, 3, 4$ require fewer multiplications than the Daubechies-9/7 wavelet. However, the filters with $N = 3, 4$ require more additions than the Daubechies-9/7 wavelet, although the filter with $N = 2$ needs fewer. Therefore, by taking both multiplication and addition into account, the computational complexity of the filters with $N = 2, 3$ is smaller than the Daubechies-9/7 wavelet, while that for $N = 4$ is almost the same. A comparison of the compression performance is shown in Table 2. It is seen that better results than the Daubechies-9/7 wavelet are obtained for almost all images. In particular, the greatest improvement is obtained for Barbara. For example, it is improved by about 1 dB at a bit rate of 1 bpp. To measure the subjective visual quality, the original and reconstructed images of Barbara are shown in Figs. 13 to 17. Almost no visual differences are found when the images reconstructed with the Daubechies-9/7 wavelet

Fig. 14. Reconstructed image with Daubechies-9/7 at 0.50 bpp (31.59 dB).

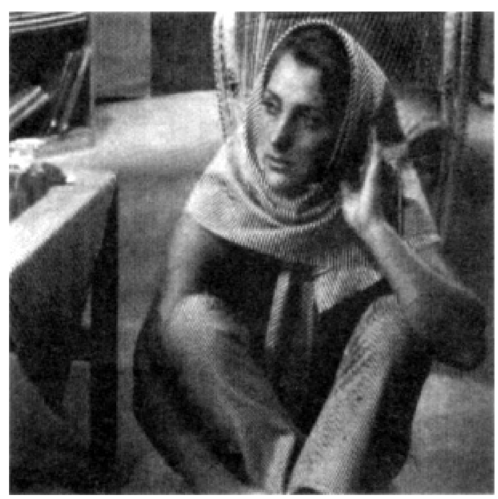

Fig. 15. Reconstructed image with All-pass-2 at 0.50 bpp (32.24 dB).

Fig. 16. Reconstructed image with All-pass-3 at 0.50 bpp (32.45 dB).

Fig. 17. Reconstructed image with All-pass-4 at 0.50 bpp (32.51 dB).

Table 3. All-pass filter's poles ($N = 2$, $K = 0$)

α_1	−0.177979816042304
α_2	−2.622020183957696

Table 4. All-pass filter's poles ($N = 3$, $K = 1$)

α_1	−0.023421767325093
α_2	−0.498798453756221
α_3	−3.334922678918686

Table 5. All-pass filter's poles ($N = 4$, $K = 0$)

α_1	−0.051223616462570
α_2	−0.407729187986630
α_3	−1.694174258880685
α_4	−9.846872936670111

and with N = 2, 3, 4 are compared. Therefore, the IIR wavelet filters with N = 2, 3, 4 proposed in this paper have a compression performance comparable to the Daubechies-9/7 wavelet. For reference, the poles of the all-pass filters with N = 2, 3, 4 are given in Tables 3 to 5, respectively.

5. Conclusions

In this paper, we have presented an effective implementation of all-pass-based IIR wavelet filters for image compression. Since IIR wavelet filters are used, both the exactly linear phase and orthonormality conditions can be simultaneously satisfied, and the filters can also be realized with smaller computational complexity. We have evaluated the IIR wavelet filters by using SPIHT to compress the practical images. We have also investigated the influence of the filter order N and the delay order K on the compression performance, and have found that the optimal K is $K = 0$ or 3 when N is even and K = 1 or 2 when N is odd. We have found from experimental results that filter orders $N = 2$ to 4 are sufficient for compression of natural images. Finally, we have shown that the IIR wavelet filters proposed in this paper have a lower computational complexity than the Daubechies-9/7 wavelet, with a comparable compression performance.

REFERENCES

1. Daubechies I. Ten lectures on wavelets. SIAM; 1992.
2. Vaidyanathan PP. Multirate systems and filter banks. Prentice–Hall; 1993.
3. Vetterli M, Kovacevic J. Wavelets and subband coding. Prentice–Hall; 1995.
4. Akansu AN, Smith MJT. Subband and wavelet transforms: Design and applications. Kluwer Academic Publishers; 1996.
5. Smith MJT, Eddins SL. Analysis/synthesis techniques for subband image coding. IEEE Trans ASSP 1990;38:1446–1456.
6. Antonini M, Barlaud M, Mathieu P, Daubechies I. Image coding using wavelet transform. IEEE Trans Image Process 1992;1:205–220.

7. Vetterli M, Herley C. Wavelets and filter banks: Theory and design. IEEE Trans Signal Process 1992;40:2207–2232.
8. Herley C, Vetterli M. Wavelets and recursive filter banks. IEEE Trans Signal Process 1993;41:2536–2556.
9. Shapiro JM. Embedded image coding using zerotree of wavelets coefficients. IEEE Trans Signal Process 1993;41:3445–3462.
10. Said A, Pearlman WA. A new, fast, and efficient image codec based on set partitioning in hierarchical trees. IEEE Trans CAS Video Technol 1996;6:243–249.
11. Selesnick IW. Formulas for orthogonal IIR wavelet filters. IEEE Trans Signal Process 1998;46:1138–1141.
12. Zhang X, Muguruma T, Yoshikawa T. Design of orthonormal symmetric wavelet filters using real all-pass filters. Signal Process 2000;80:1551–1559.
13. Adams MD, Kossentini F. Reversible integer-to-integer wavelet transforms for image compression: Performance evaluation and analysis. IEEE Trans Image Process 2000;9:1010–1024.

AUTHORS (from left to right)

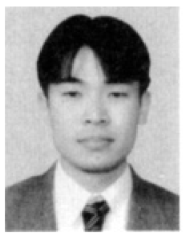
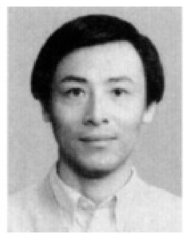


Seiya Kamimura received his B.E. degree in electrical engineering from Nagaoka University of Technology in 1999 and is currently pursuing his M.E. degree. His research interest is wavelets.

Xi Zhang received his B.E. degree in electronics engineering from Nanjing University of Aeronautics and Astronautics (NUAA) in 1984, and M.E. and Ph.D. degrees in communication engineering from the University of Electro-Communications (UEC) in 1990 and 1993. He was with the Department of Electronics Engineering at NUAA from 1984 to 1987, and the Department of Communications and Systems at UEC from 1993 to 1996, all as an assistant professor. Since 1996, he has been with the Department of Electrical Engineering of Nagaoka University of Technology as an associate professor. He was a recipient of the Award of Science and Technology Progress of China in 1987. His research interests are in the areas of digital signal processing, filter design theory, filter banks and wavelets, and applications to image coding. He is a senior member of IEEE.

Toshinori Yoshikawa received his B.E., M.E., and D.Eng. degrees from Tokyo Institute of Technology in 1971, 1973, and 1976. From 1976 to 1983, he was with Saitama University engaging in research on signal processing and its software development. Since 1983, he has been with Nagaoka University of Technology, and is currently a professor. His main research area is digital signal processing. He is a member of the IEEE Computer Society.